Phase identification of individual crystalline particles by electron backscatter diffraction (EBSD)

J. A. Small* & J. R. Michael †

*National Institutes of Standards and Technology, Gaithersburg, MD 20899-8371, † Sandia National Laboratories, Albuquerque, NM 87185-1405

Summary

Recently, an EBSD system was developed that uses a 1024 x 1024 CCD camera coupled to a thin phosphor. This camera has been shown to produce excellent EBSD patterns. In this system, crystallographic information is determined from the EBSD pattern and coupled with the elemental information from energy or wavelength dispersive x-ray spectrometry. Identification of the crystalline phase of a sample is then made through a link to a commercial diffraction database. To date, this system has been applied almost exclusively to conventional, bulk samples that have been polished to a flat surface. In this investigation, we report on the application of the EBSD system to the phase identification analysis (PIA) of individual micrometer and submicrometer particles rather than flat surfaces.

1. Introduction

Electron backscatter diffraction (EBSD) patterns were first observed by Alam *et al.* (1954). Venables & Harland (1973) made the initial observation of EBSD in the scanning electron microscope (SEM) with a video-rate-camera detection system. This system used a phosphor screen that was imaged by a low-light-level video-rate camera. Since that time fast, automated EBSD systems have been developed for rapid microstructural characterization, e.g., mapping of

DISCLAIMER

the crystallographic orientation of microscopic grains and grain boundaries of bulk samples. Grain orientation studies currently represent the most widely used applications for EBSD. The reader is referred to the Journal of Microscopy, Volume 195, part 3, September 1999 for an excellent discussion of this and related applications.

Goehner & Michael (1996) developed an EBSD system that used a high-gain 1024 x 1024 CCD camera directly coupled by a fiber optic reducer to a phosphor screen. Unlike previous EBSD systems which were designed primarily for determining microstructural information such as the grain orientation in bulk samples, this system was specifically designed to identify the crystalline phase of unknown materials. In their system, the quality of the EBSD pattern was significantly improved over earlier systems not only by the high gain of the camera but also by the development of a background correction (flat-fielding) method to compensate for the strong angular dependence of the backscattered electrons. The flat-fielding correction consists of dividing on a pixel-by-pixel basis the original image by a reference image that represents only the general scattering distribution that would be obtained from an amorphous material with the same average atomic number. Automated pattern analysis was carried out using a Hough transform to locate band positions and band widths in the pattern and hence the interplanar spacing Leavers (1992) and Lassen *et. al* (1992). This information along with the angles between the bands was used to determine sub-cell volumes where the unit cell volume is an integer multiple of the sub-cell volume. Next this crystallographic information was combined with the elemental information from energy or wavelength dispersive x-ray spectrometry to search a diffraction database for possible matching phases. In their system the authors used the Powder

Diffraction Files published by the International Center for Diffraction Data (ICDD)[1]. Once a given phase was identified an EBSD pattern was synthesized with the correct orientation and overlaid on the EBSD pattern of the unknown for comparison, Michael *et. al* (1998). Their phase identification analysis (PIA) system offered one of the first practical systems for rapid identification of the crystallographic phase of unknowns in the SEM. EBSD/PIA was first applied to conventional, bulk polished samples, Medevielle, *et. al* (1999). In this investigation, we examined the feasibility of using the EBSD/PIA system for single-particle analysis of micrometer and submicrometer-sized particles.

2. Experimental

For this study we analyzed a series of particles with known elemental compositions. These particles included U_3O_8 (NIST SRM #U900), PbO_2, SiC, Al_2O_3, PbS (galena) and $PbMoO_4$ (wulfenite). Particles from each of the materials were dispersed onto pyrolitic carbon substrates or double-stick carbon tape and were uncoated except for the galena particles which were coated with less than 10 nm of C. The acceleration potential was 20 keV and the substrate was tilted at an angle of 70 degrees to the horizontal towards the EBSD camera. The samples were analyzed either at Sandia National Laboratories in a JEOL 6400 SEM[2] equipped with a custom built CCD camera that has been described previously Goehner & Michael (1996), or at NIST in a Hitachi S-4500 field emission SEM equipped with a NORAN 32 bit Phase ID System.

---

[1] Published by the International Center for Diffraction Data, Powder Diffraction File, Newtown Square, PA.

[2] Certain commercial equipment, instruments, or materials are identified in this report to specify adequately the experimental procedure. Such identification does not imply recommendation or endorsement by the National Institute of Standards and Technology, nor does it imply that the materials or equipment identified are necessarily the best available for the purpose.

3. Results and Discussion

Initially, we used two of the particles standards, reagent grade PbO_2 and NIST SRM #U900, both with relatively small particle-size distributions and high average atomic numbers to determine the feasibility of using EBSD/PIA for single-particle analysis. The results of the EBSD/PIA of a 0.5 μm lead oxide and a 0.3 μm uranium oxide particle are shown in Figs. 1 and 2 respectively. Each figure contains a secondary electron image of the analyzed particle (a), a background-corrected EBSD pattern (b), and the synthesized pattern overlaid on the EBSD pattern (c). Considering the small particle size, the diffraction pattern obtained from the lead oxide particle, Fig. 1b, has an excellent signal-to-noise ratio, comparable to the quality obtained from a flat, bulk target. The results from the PIA of the particle identified it as plattnerite, PbO_2, (powder diffraction file # 41-1492), Small & Michael (1999). Figure 2 shows the results from the PIA of the uranium oxide particle. As in the case of the PbO_2 particle, the quality of the diffraction image for the U-containing particle is excellent and the particle was easily identified as orthorhombic U_3O_8 (powder diffraction file # 24-1172). The results of this first attempt at PIA of single particles indicate that phase identification is possible on submicrometer particles. In addition, the high quality of the diffraction images from these particles implied that at least for high Z materials such as these it may be possible to obtain usable EBSD patterns from particles 100 nm or smaller in size.

Although we were successful at our initial efforts to identify the phase of single particles by EBSD, in a more general sense the PIA of individual particles may be complicated by factors related to particle geometry and size. As part of this initial study we looked at three of these factors that included:

1. The ability to obtain appropriate background/ flat-field reference images for individual particles.

2. The effects of particle size on EBSD image quality and pattern interference from nearby particles or substrates.

3. The effects of particle composition/average atomic number on EBSD image quality.

Background correction/Flat-Field Processing

The angular modulation of backscattering caused by EBSD diffraction effects rides upon the general angular distribution of backscattering from the sample. At normal beam incidence, that distribution closely follows a cosine function relative to the surface normal and is rotationally symmetric around the normal. At the high tilt angles (~ 70 degrees from the normal) required for efficient EBSD detection, the angular distribution of backscattering is highly peaked in the forward scattering direction, approximately around the specular reflection of the incident beam as shown in Fig. 3. Moreover, the scattering is maximized horizontally in the plane defined by the incident beam vector and the surface normal. In EBSD analysis, the dynamic signal range due to diffuse backscattering shown in Fig. 4b overwhelms the weak crystallographic/EBSD pattern to the point where the EBSD pattern is barely visible in Fig. 4c requiring an accurate procedure to extract the weak, diffraction image from the combined, raw image. In this study we used the flat-fielding correction as mentioned above.

For a flat sample, a background image can be readily obtained (e.g., for a polycrystalline target, the beam can be scanned over several grains, randomizing the crystallographic contrast). As long as the sample composition (which affects total backscattering) and the position relative to the incident beam and the camera are maintained constant so that the image centroids are the same for the background and EBSD images, the same reference image can be used for an entire sample or sample set. Alternatively, Prior *et. al* (1999) have developed background correction schemes based on local averaging of the pixels in the raw EBSD image and Noran has developed a procedure to compensate for differences in total backscattering between the image used for the background and the EBSD image by using an auto exposure setting to adjust the gray-levels of the background and raw EBSD images so that they are approximately the same.

Consider the case for a particle, as illustrated in Fig. 5, which shows the vertical and horizontal position of the centroid for the backscattered electron distribution for different beam positions on a spherical particle. Figure 5a illustrates the vertical positioning of the image centroid that can be defined by the specular reflection of the incident beam from a line tangent to the particle at the point of beam impact. Figure 5b illustrates the corresponding horizontal positioning of the image centroid defined by the incident beam vector and the local surface normal, which changes drastically as the beam is placed at different locations on the particle surface. In the case of the spherical particle, the effective tilt angle depends on the exact location of the beam impact. The angular distribution for the EBSD image would be aligned with the reference image, collected

from a flat sample tilted at 70 degrees, only at a beam location where the alignment between the beam, the particle surface and the surface normal corresponds to the same relative alignment as the flat-fielding reference. The greater the difference between the angular distribution of the background and particle EBSD pattern images, the less effective the flat-fielding procedure and the lower the quality of the EBSD pattern.

For lack of a defined flat-fielding procedure for individual particles, we decided to obtain background images using a method similar to the method described for flat samples by scanning the beam over features where the crystallographic contrast is randomized. For the large galena particle shown in Fig. 4, the background image was obtained by scanning the beam over an area of the particle where there was a fracture exposing several surfaces with multiple orientations relative to the camera face. This is shown in Fig. 4a where the X indicates the acquisition location for the EBSD image, the square indicates the acquisition location of the background image and the camera is positioned, with respect to the image, in the direction of the upper left corner. The two images, Figs. 4b and 4c, show a slight shift in the centroid indicated by the "o" and "x" marked on the images. In the background image, Fig. 4b, the "o" marks the centroid of the scattering distribution for Fig. 4b and the "x" marks the centroid for the EBSD image Fig. 4c. Similarly in Fig. 4c the "o" marks the centroid for Fig. 4c and the "x" the centoid for Fig. 4b. For this example, the shift was small enough that the background correction resulted in the excellent EBSD image shown in Fig. 4d.

For smaller particles flat-field images were acquired by scanning over small groupings of particles adjacent to the one being analyzed for PIA. Figure 6a shows an example of a processed EBSD pattern from a 1.3 micrometer-sized PbO_2 particle where the reference flat-field image was obtained by scanning the beam over a nearby cluster of PbO_2 particles similar to the cluster shown in Fig. 6b.

Although the simple background-correction procedures discussed in the preceding paragraphs worked reasonably well for the examples tested, the selection of the exact measurement location for the background and the EBSD image to minimize the difference in angular distributions of the backscttered electrons may dramatically affect the success rate for successful PIA of single particles particularly those less than a micrometer in size. Experimental work is continuing to define better reference images and "flat-fielding" correction procedures for particles.

Effects of Particle Size

The large number of electrons, both elastic and inelastic, that are scattered out the sides of, or penetrate through small particles, particularly particles less than about one micrometer in size, can significantly affect the quality of the final EBSD image. Scattered electrons may interact with an amorphous mounting substrate adding to the general background intensity and reducing the signal-to-noise ratio in the EBSD image. Scattered electrons may exit the particle volume without diffracting but may then interact with the substrate (if it is crystalline) or an adjacent particle and then generate an interfering EBSD pattern. Evidence of scattered electrons from

small particles is shown in Fig. 7. Figure 7(a) is the secondary electron image of a pair of SiC grains, where a small grain approximately 2 μm in size rests on top of a much larger one. Figure 7(b) is the pattern from the smaller particle and 7(c) is the EBSD pattern from the large particle. A close inspection of the EBSD image from the small particle shows the presence of faint lines, three of which have been marked, corresponding to lines in the pattern of the large underlying particle. The presence of the faint lines from the large grain in the EBSD image of the small grain, we believe, is from the diffraction of electrons in the large particle that were initially elastically scattered out of the smaller particle volume probably through the sides. The loss of these electrons, which would normally diffract from the region of interest in a conventional sample, adversely affects the EBSD pattern from the particle of interest in two ways. First, the loss of the elastically scattered electrons results in a lower diffracted signal and hence a poorer quality EBSD image from the particle of interest. Second, the elastically scattered electrons diffract from the alternate source, in this case the large SiC particle, resulting in extra lines in the pattern image from the particle of interest. These extra lines may make it difficult or in some cases impossible to correctly index the pattern from the particle of interest.

In course of our study of the effects of particle size on the quality of the EBSD images, another aspect of small particle analysis we observed was a general reduction in image quality for many of the particles 1 μm and below in size which could not be explained totally by electron scattering. For example, Figure 8 shows the EBSD images collected from three wulfenite particles 1,10, and 100 μm in size. The quality of the EBSD images, as estimated qualitatively by the intensity/contrast, total number, and sharpness of the Kikuchi lines, improves significantly from the 1 μm to the 10 μm particle and is similar for the 10 μm and 100 μm particles. Although

the quality of the EBSD image for the 1 μm particle is sufficient for PIA, the earlier experience with the submicrometer particles discussed above suggests that the image quality of the 1 μm wulfenite particle should have been higher. This implies that in addition to electron scattering, image quality for smaller particles may also be influenced by other factors such as surface damage, materials properties, particle shape, and sample orientation. Additional studies are required to understand better the factors that influence the EBSD image quality for particles.

The effects of particle composition/average atomic number on EBSD image quality.

Figure 9 is a plot of the bulk-target backscattered electron yield as a function of atomic number Z. The backscatter yields were calculated using the NIST multi-scattering Monte Carlo routine for a 20 kV accelerating potential and targets tilted at 70 degrees, Newbury & Myklebust (1995). The plot shows that the number of backscattered electrons produced in a given sample is highly dependent on the sample average atomic number or composition with high-Z materials having a significantly greater number of backscattered electrons than low-Z materials. The implication for the PIA of particles is that the quality of EBSD images from relatively low-Z particles will be poor compared to the image quality from similar-sized relatively high-Z particles. Figure 10 shows the EBSD images collected from a 0.3 μm Al_2O_3 particle (Figure 10a) and the 0.3 μm U_3O_8 particle (Figure 10b) from Figure 2. The overall image quality from the Al_2O_3 particle is poor with the Kikuchi lines barely visible above background. The quality of this image is not sufficient to perform a PIA. In contrast, the U_3O_8 particle image was easily indexed and the phase of the particle was identified as orthorhombic U_3O_8.

The observed difference in pattern quality between the Al_2O_3 and U_3O_8 particles may also be explained by the difference in the density between Al_2O_3 at 4.0 compared to U_3O_8 at 8.3. The lower density for the Al_2O_3 means the electron range in this material is quite large compared to U_3O_8, allowing many of the electrons to penetrate through the particle into the substrate. As mentioned previously, this decreases the diffraction signal and increases the average background in the EBSD pattern, decreasing the overall pattern contrast to an unacceptably low level.

As mentioned above additional studies are required to understand better the factors that influence the EBSD image quality for particles. The step to help resolve these two effects will be to analyze particles mounted on thin carbon films to minimize the signal originating from the substrate.

4. Conclusions

Backscattered electron diffraction combined with phase identification software was successfully used to identify the crystalline phase of single particles as small as 0.3 μm in diameter. Initial studies were conducted on known particles to determine the effects of particle shape and size/mass on various procedures associated with PIA. The results of these studies showed:

1. Background correction procedures were successful for many of the particles analyzed in this study. These procedures, however, will probably require additional refinements for general application to the PIA of individual particles.
2. Electron scattering, both elastic and inelastic, resulted in lower quality EBSD images for particles less than about 1 μm in size.

3. The EBSD pattern quality for a given particle size will be dependent on the particle composition, with lower Z materials requiring significantly larger particles for PIA compared to higher Z materials.

In general our experience was that the EBSD-PIA system was very successful in identifying the phases of the analyzed particles. This system used in conjunction with an analytical SEM or EPMA provides the analyst with a very powerful and straightforward method to obtain an absolute identification of submicrometer and larger crystalline particles.

References

Alam, M.N., Blackman, M. & Pashley, D.W. (1954) High angle Kikuchi patterns. *Proc. R. Soc. London Ser.* **221A**, 224-242.

Goehner, R.P., & Michael J.R., (1996) Phase identification in a scanning electron microscope using backscattered electron Kikuchi patterns. *J. Res. Natl. Inst. Stand. Technol.* **101**, 301-308.

Krieger Lassen, N.C., Juul Jensen, D. & Conradsen, K. (1992) Image processing procedures for analysis of electron backscatter patterns. *Scanning Micros.*, **6**, 115-121.

Leavers, V.F. (1992) *Shape Detection in Computer Vision Using the Hough Transform*, Springer-Verlag, New York.

Medevielle, A., Hugon, I., & Dugne O. (1999) Electron backscatter diffraction: Applications for nuclear materials. *J. Micros.*, **195**, 233-238.

Michael, J.R., Schlienger, M.E., & Goehner, R.P. (1997) Electron backscatter diffraction in the SEM: is electron diffraction in the TEM obsolete? *Micros. & Microanal.*, **3** Supp. 2, 879-880.

Prior, D.J., Boyle, A.P., Brenker, F., Cheadle, M.C.,Day, A., Lopez, G., Peruzzo, L., Potts, G.J., Reddy, S., Spiess, R., Timms, N.E., Trimby, P., Wheeler, J., & Zetterstrom, L. (1999) The application of electron backscatter diffraction and orientation contrast imaging on the SEM to textural problems in rocks. *Am. Mineral.*, **84**, 1741-1759.

Newbury, D.E., Myklebust R.L., & Swyt, C.R. (1995) The use of simulated standards in quantitative electron probe microanalysis with energy-dispersive x-ray spectrometry *Microbeam Analysis*, **4**, 221-238.

Small, J.A., & Michael, J.R., (1999) Phase identification of individual particles by electron backscatter diffraction (EBSD) *Micros. & Microanal.*, 5 Supp. 2, 226-227.

Venables, J.A. & Harland, C.J. (1973) Electron backscattering patterns. A new technique for obtaining crystallographic information in the scanning electron microscope. *Philos. Mag.* **27**, 1193-1200.

---

*JRM was supported by the United States Department of Energy under Contract DE-AC04-94AL85000. Sandia is a multiprogram laboratory operated by Sandia Corporation, a Lockheed Martin Company, for the United States Department of Energy.

Figure Captions

Fig. 1. PIA of a 0.5 μm PbO_2 particle. (a) Secondary electron image of the particle. (b) Background-corrected EBSD pattern. (c) Indexed EBSD pattern with simulated pattern overlay.

Fig. 2. PIA of a 0.3 μm U_3O_8 particle. (a) Secondary electron image of the particle. (b) Background-corrected EBSD pattern. (c) Indexed EBSD pattern with simulated pattern overlay.

Fig. 3. Electron backscatter distribution from a flat sample.

Fig. 4. Images showing the flat-field correction for a 100 μm galena particle. (a) Secondary electron image of galena particle. The X marks the collection location of the EBSD image and the square the collection location of the background image. (b) Flat-field background image. The "o" marks the centroid for this image the "x" marks the centroid for image 4c. (c) Uncorrected EBSD image. The "o" marks the centroid for this image the "x" marks the centroid for image 4b. (d) EBSD image after flat-field correction.

Fig. 5. Distribution of the backscattered electron image centroid from a spherical particle. (a) Vertical distribution of the backscattered electrons. (b) Horizontal distribution of the backscattered electrons.

Figure Captions

Fig. 1. PIA of a 0.5 μm PbO_2 particle. (a) Secondary electron image of the particle. (b) Background-corrected EBSD pattern. (c) Indexed EBSD pattern with simulated pattern overlay.

Fig. 2. PIA of a 0.3 μm U_3O_8 particle. (a) Secondary electron image of the particle. (b) Background-corrected EBSD pattern. (c) Indexed EBSD pattern with simulated pattern overlay.

Fig. 3. Electron backscatter distribution from a flat sample.

Fig. 4. Images showing the flat-field correction for a 100 μm galena particle. (a) Secondary electron image of galena particle. (b) Flat-field background image. (c) Uncorrected EBSD image. (d) EBSD image after flat-field correction.

Fig. 5. Distribution of the backscattered electron image centroid from a spherical particle. (a) Vertical distribution of the backscattered electrons. (b) Horizontal distribution of the backscattered electrons.

Fig. 6. EBSD pattern from a 1.3 μm PbO particle. (a) EBSD pattern after flat-field correction. (b) Cluster of PbO_2 particles similar to that used for the background image in the flat-field correction for 6(a).

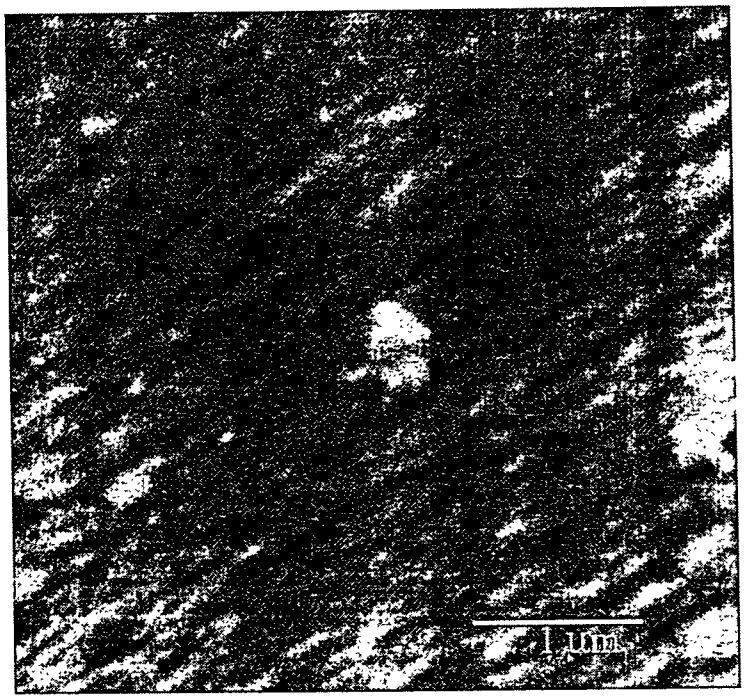
1 μm

(a)

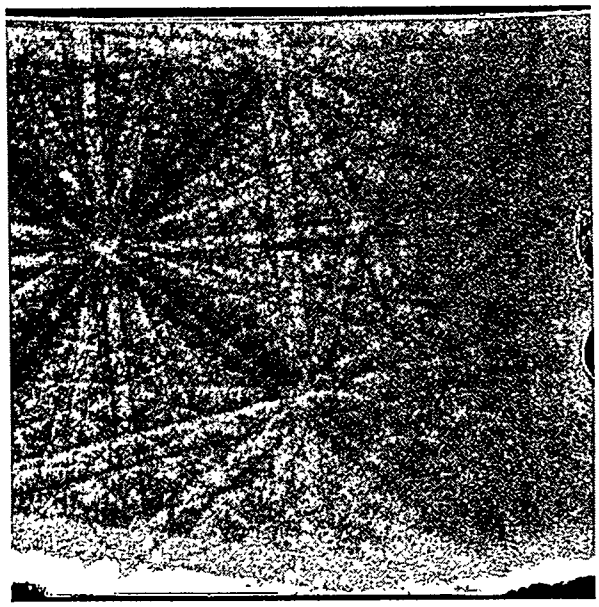

(b)

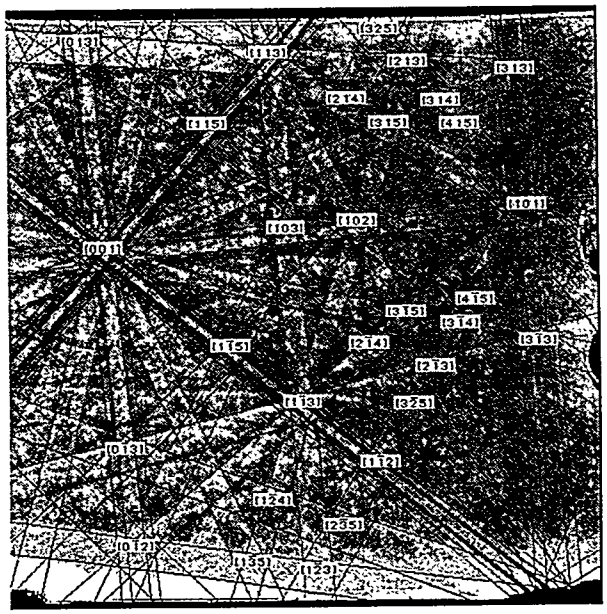
[0 1 3]
[1 1 3]
[3 2 5]
[2 1 3]
[3 1 3]
[2 1 4]
[3 1 4]
[1 1 5]
[3 1 5]
[4 1 5]
[1 0 1]
[1 0 3]
[1 0 2]
[0 0 1]
[4 1 5]
[3 1 5]
[3 1 4]
[1 1 5]
[2 1 4]
[3 1 3]
[2 1 3]
[1 1 3]
[3 2 5]
[0 1 3]
[1 1 2]
[1 2 4]
[2 3 5]
[0 1 2]
[1 3 5]
[1 2 3]

(c)

Fig.1

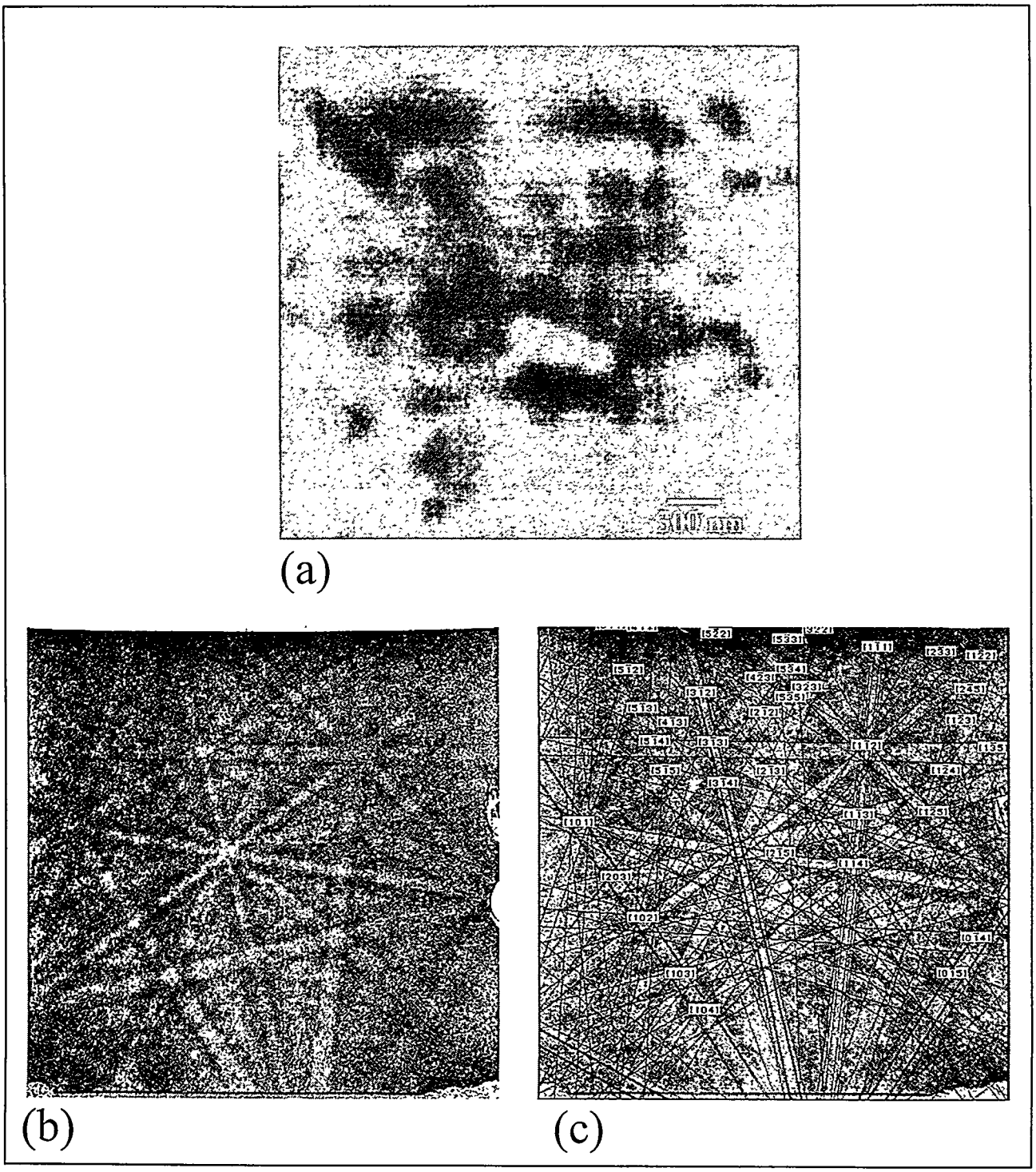

Fig. 2

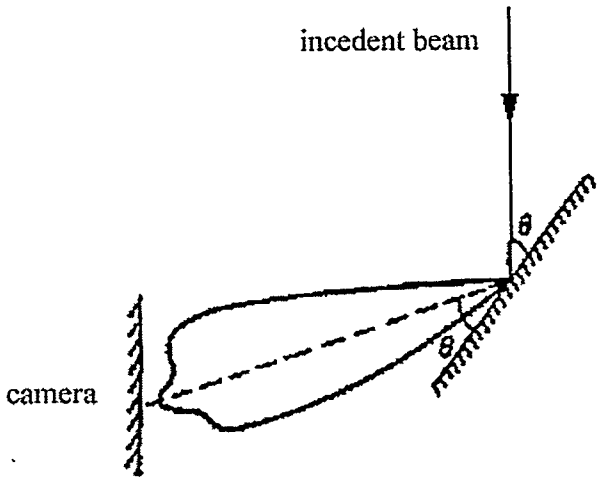

Fig. 3

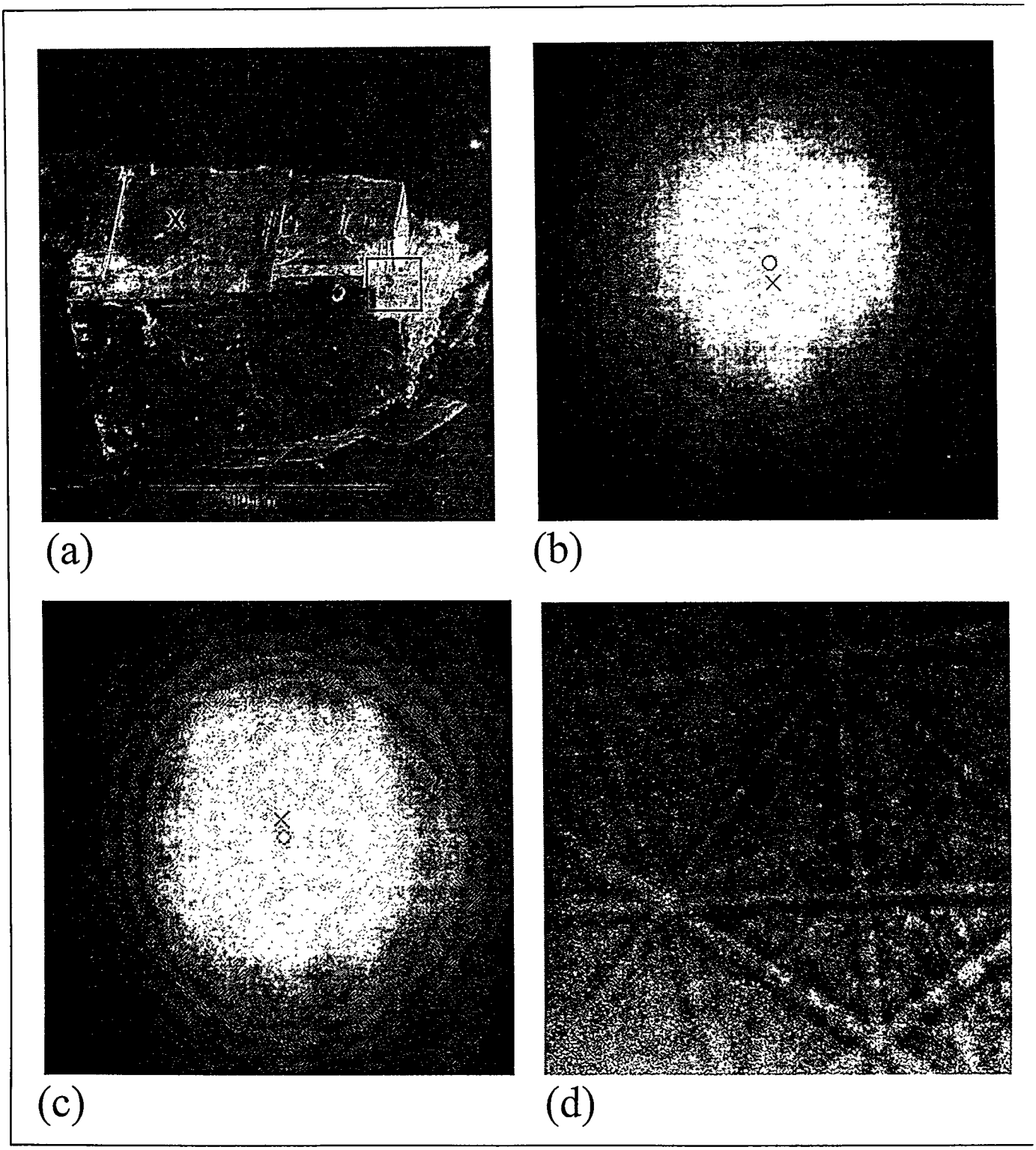

Fig. 4

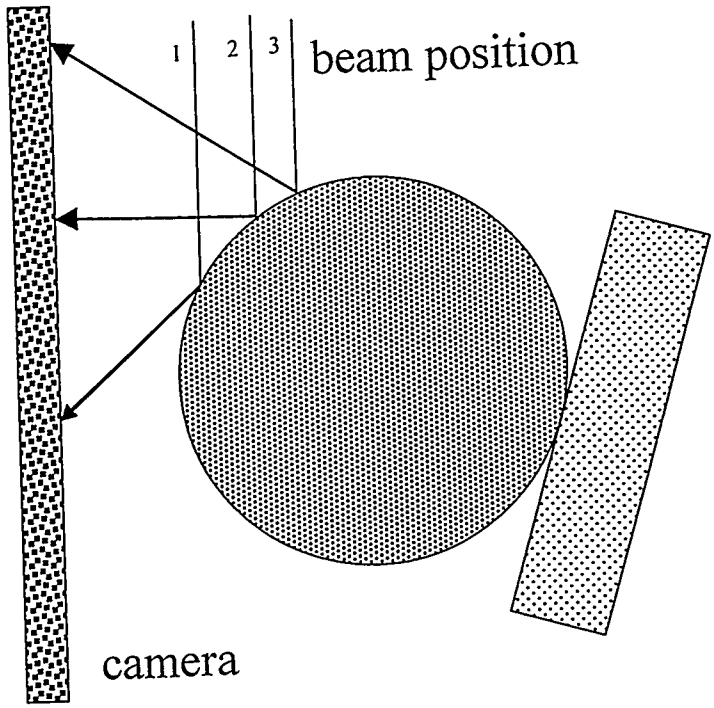

(a)

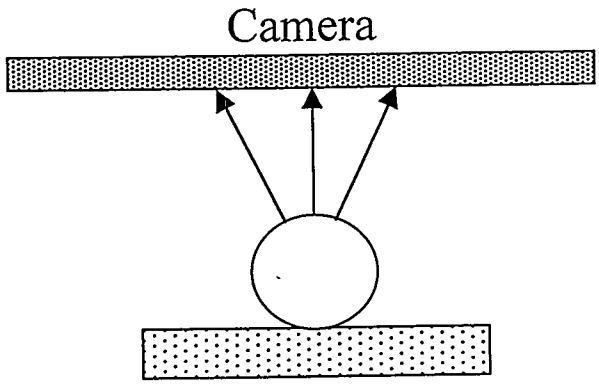

(b)

Fig. 5

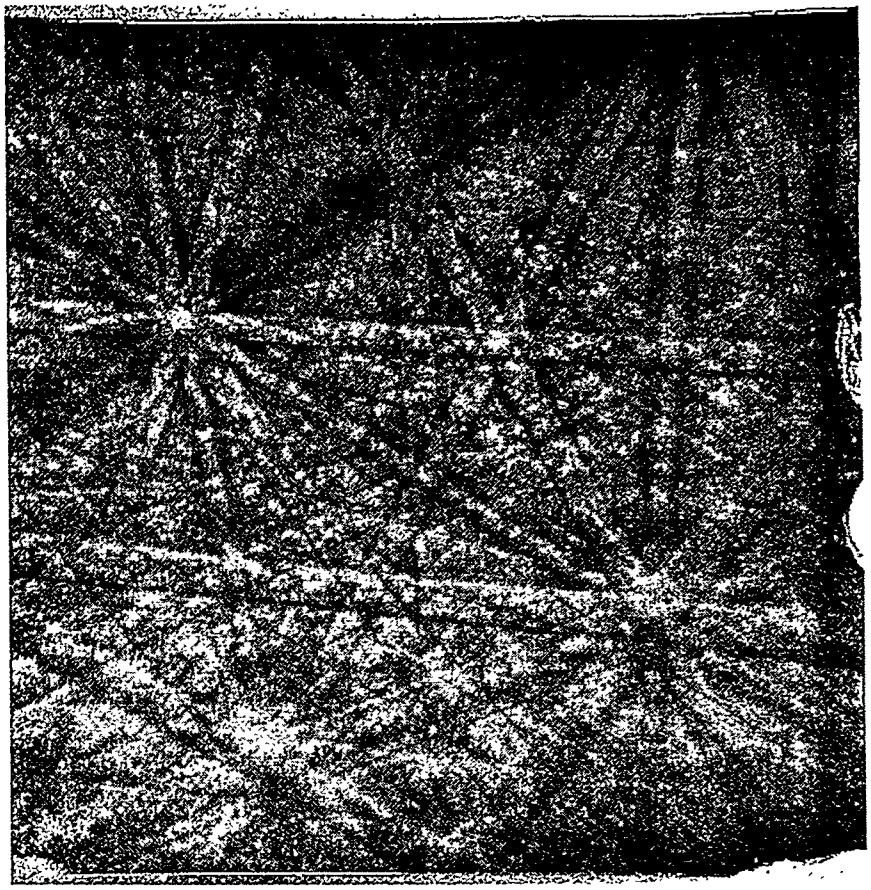

(a)

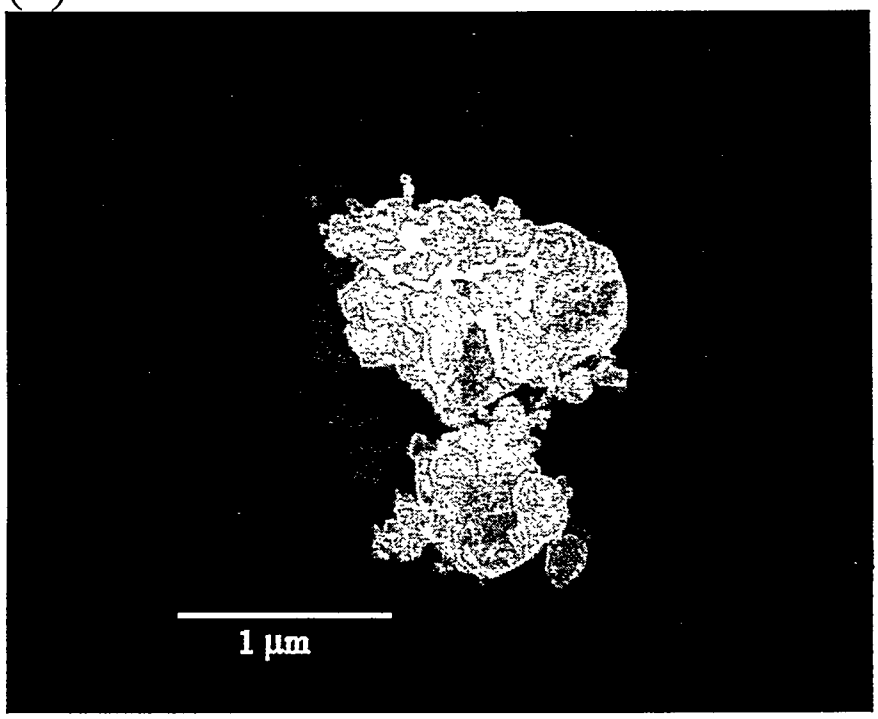

(b)

Fig. 6

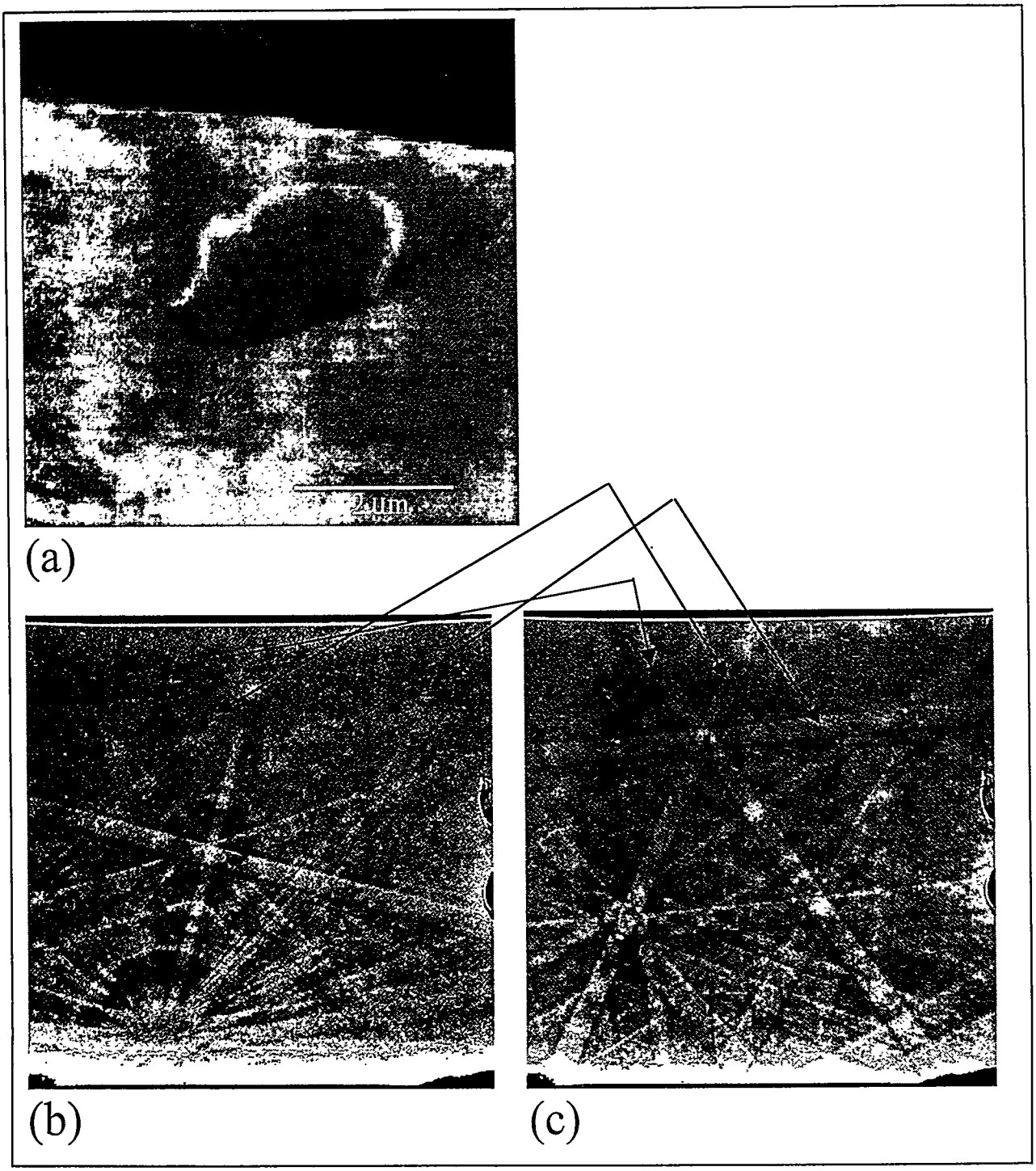

Fig. 7

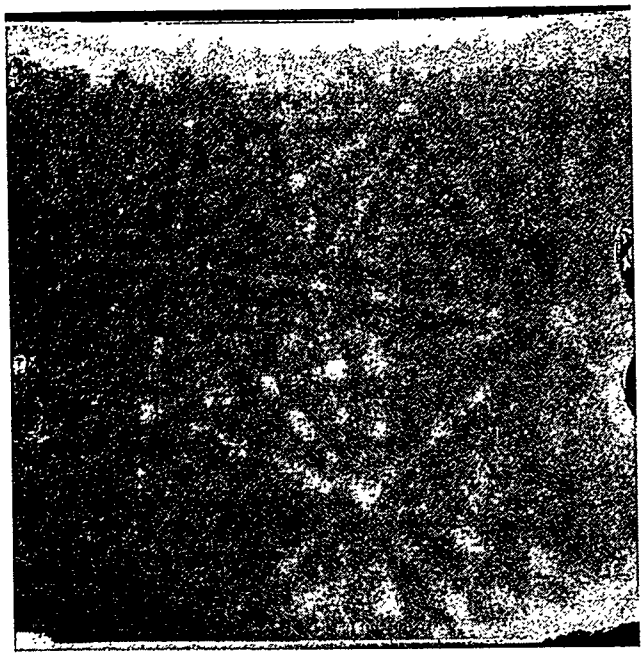

(a)

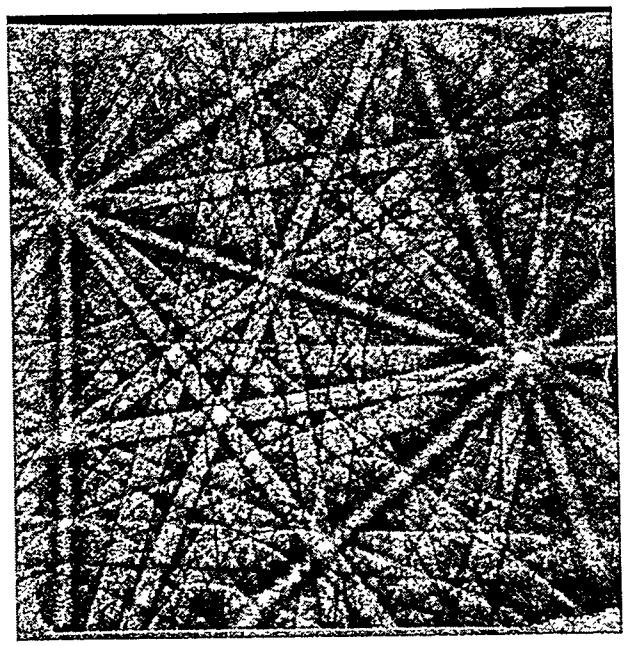

(b)

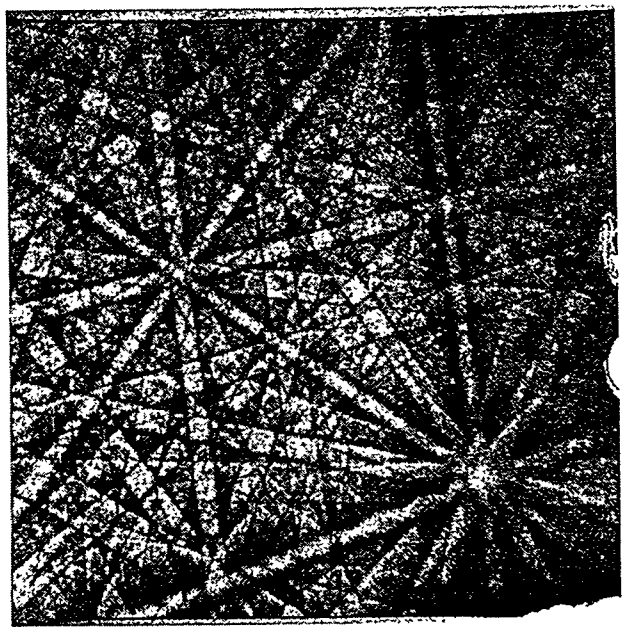

(c)

Fig. 8

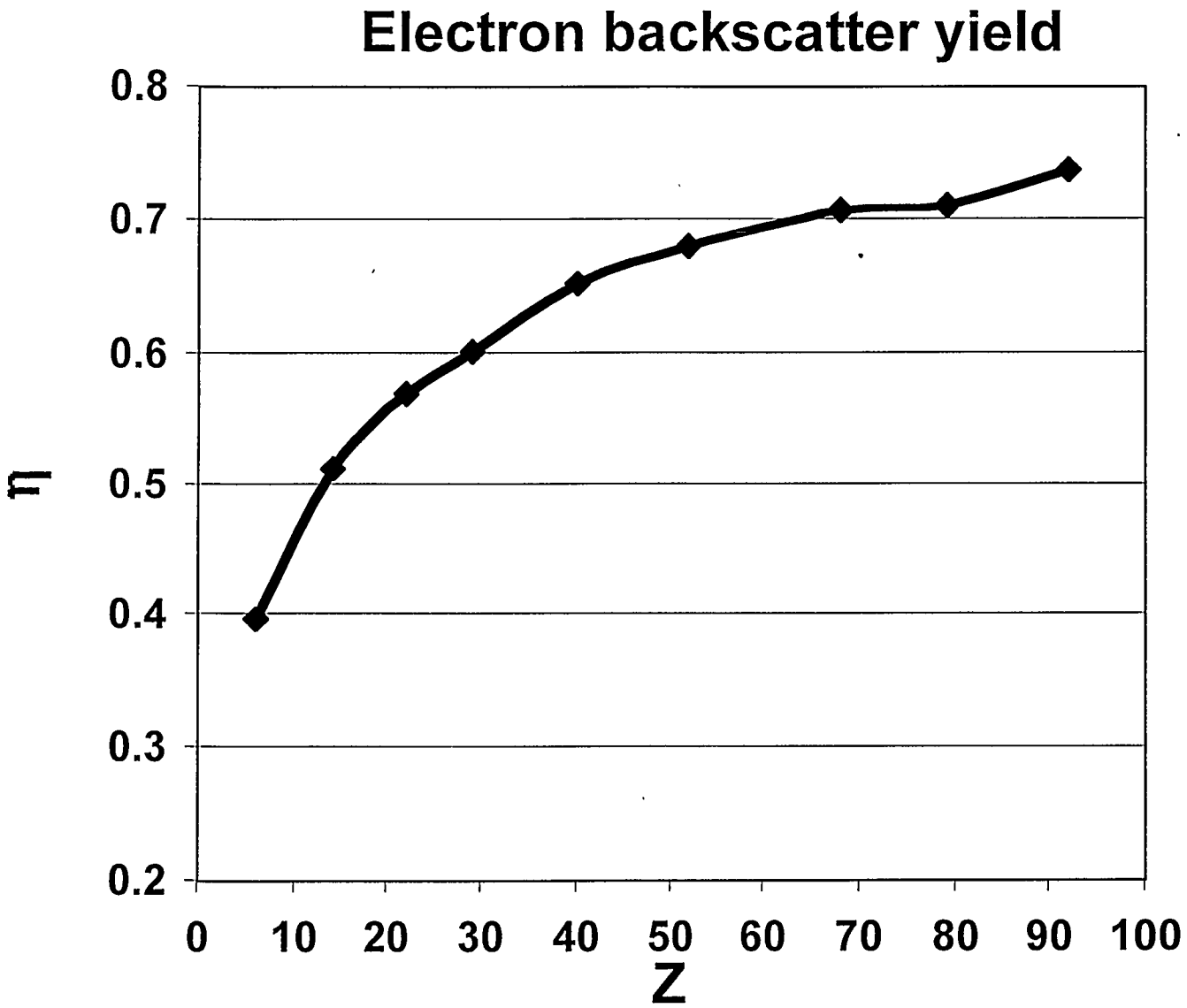
Electron backscatter yield
0.8
0.7
0.6
0.5
0.4
0.3
0.2
η
0
10
20
30
40
50
60
70
80
90
100
Z

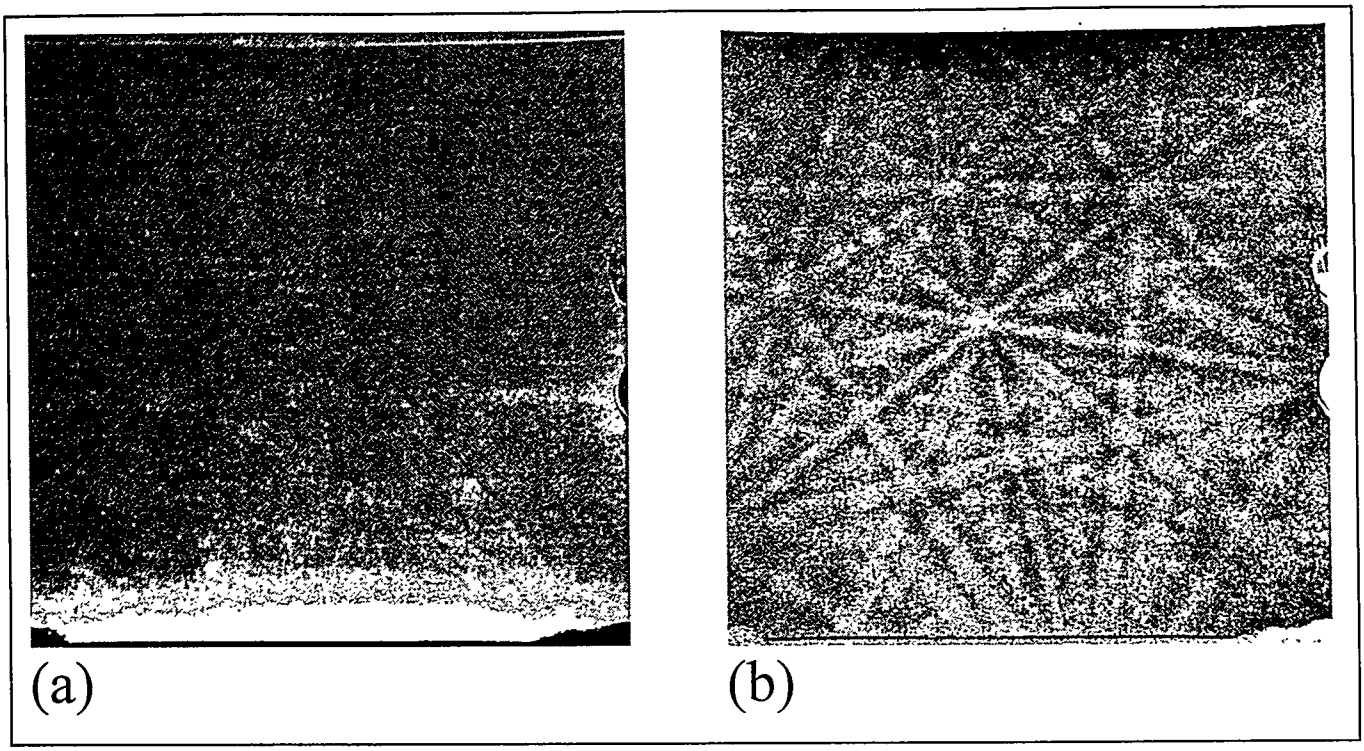

Fig. 10